ACS APPLIED MATERIALS & INTERFACES

Research Article

www.acsami.org

Polymer-Ag Nanocomposites with Enhanced Antimicrobial Activity against Bacterial Infection

Lin Mei,[†] Zhentan Lu,[†] Xinge Zhang,*[,†] Chaoxing Li,*[,†] and Yanxia Jia[‡]

[†]Key Laboratory of Functional Polymer Materials of Ministry Education, Institute of Polymer Chemistry, Nankai University, Tianjin 300071, China

[‡]National Laboratory of Biomacromolecules and Center for Biological Electron Microscopy, Institute of Biophysics, Chinese Academy of Sciences, Beijing 100101, China

Supporting Information

ABSTRACT: Herein, a nontoxic nanocomposite is synthesized by reduction of silver nitrate in the presence of a cationic polymer displaying strong antimicrobial activity against bacterial infection. These nanocomposites with a large concentration of positive charge promote their adsorption to bacterial membranes through electrostatic interaction. Moreover, the synthesized nanocomposites with polyvalent and synergistic antimicrobial effects can effectively kill both Gram-positive and Gram-negative bacteria without the emergence of bacterial resistance. Morphological changes obtained by transmission electron microscope observation show that these nanocomposites can cause leakage and chaos of intracellular contents. Analysis of the antimicrobial mechanism confirms that the lethal action of nanocomposites against the bacteria started with disruption of the bacterial membrane, subsequent cellular internalization of the nanoparticles, and inhibition of intracellular enzymatic activity. This novel antimicrobial material with good cytocompatibility promotes healing of infected wounds in diabetic rats, and has a promising future in the treatment of other infectious diseases.

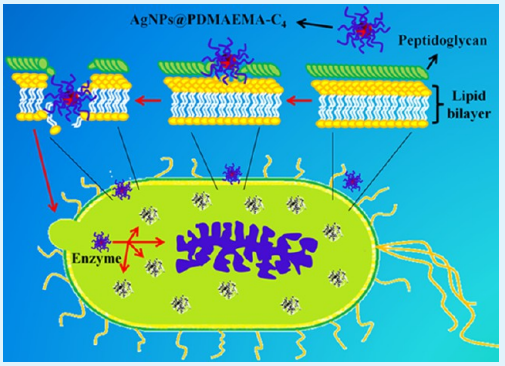

KEYWORDS: *antibacterial material, cationic polymers, silver nanoparticles, wound healing, bacterial infection*

INTRODUCTION

Infections from antibiotic-resistant bacteria pose a significant threat to human health worldwide. In the United States alone, more than 2 million people with antibiotic-resistant infections are reported every year, with at least 23 000 deaths as a result.[1] These bacteria are extremely resistant to conventional antibiotics owing to acquired resistance, limited diffusion, and intracellular inactivation. Therefore, the development of new antimicrobial materials with high safety and antibacterial activity and without bacterial resistance is crucial.

Cationic polymers that possess a high number of positive charges and membrane-disrupting activity toward negatively charged microbial surface phospholipids show potent antimicrobial activity against bacteria, fungi, and viruses.[2] To acquire permanent antibacterial properties, most cationic polymers are immobilized onto the substrate surface or made into hydrogels.[3,4] However, their antimicrobial activities may be obviously reduced because penetration of the cell membranes into the cytoplasm is limited during immobilization.[5] Nanomaterials, which are capable of diffusing into the bacterial membrane and disrupting its integrity, provide a new opportunity for the antimicrobial application of cationic polymers. Silver nanoparticles (AgNPs), one of the predominant nanomaterials, display broad-spectrum antimicrobial activity against bacterial and fungal species, including antibiotic-resistant strains. AgNPs are used for the treatment of burns and marketed as a water disinfectant and room spray.[6] Combination of AgNPs with cationic polymers facilitates constant stability of dispersed AgNPs in aqueous solution. This nanocomposite easily forms core−shell structured nanoparticles with an AgNP core and cationic polymer shell with the alkyl tail arranged toward the surrounding environment. The formation of nanoparticles is expected to increase the local density of the positive charge and promote its adsorption to negatively charged bacterial membranes through electrostatic interactions, thereby enhancing antimicrobial property and diffusivity into the bacterial membrane. In addition, this nanoparticle with two biologically active fragments, combined with the goal of merging different modes of action synergistically, is optimal for wound healing. Notably, the convergence of two antimicrobial materials into a single one does not appear to induce bacterial resistance.

Herein, we synthesized a new antibacterial nanoparticle with a tertiary amino group containing the monomer 2-(dimethylamino)ethyl methacrylate (DMAEMA), which was directly polymerized via reversible addition−fragmentation chain transfer (RAFT) polymerization. The PDMAEMA chains were quaternized with alkyl bromide in the tertiary amino

Received: May 13, 2014
Accepted: August 29, 2014
Published: August 29, 2014

   dx.doi.org/10.1021/am502886m | ACS Appl. Mater. Interfaces 2014, 6, 15813−15821

groups (PDMAEMA-C_n, n = 2, 4, 8, 12, and 16, and similarly hereafter) and subsequently used as templates to prepare cationic polymer PDMAEMA-C_n-stabilized AgNPs (AgNPs@PDMAEMA-C_n). To achieve desired antimicrobial activity and cytocompatibility, the synthesis conditions (e.g., different alkyl chains, molar ratio of PDMAEMA-C_n and silver, the volume of reducing agent, and the molecular weight of PDMAEMA-C_n) of AgNPs@PDMAEMA-C_n were optimized comprehensively. Moreover, the synthesis, characterization, antibacterial activity, antibacterial mechanism, and biocompatibility of AgNPs@PDMAEMA-C_n were systematically studied. Finally, we further explored the effects of new antimicrobial materials on the treatment of bacteria-induced wound infection in healthy and diabetic rats.

EXPERIMENTAL DETAILS

Preparation of AgNPs@PDMAEMA-C_4. Typically, 102 μL of 10 mg/mL (58.8 mmol/L) $AgNO_3$ and 214 μL of 300 mg/mL (28.0 mmol/L) PDMAEMA-C_4 (molar ratio 1:1) were mixed with 4.53 mL of methanol under vigorous stirring in an ice−water bath. Then, 150 μL of 11.8 mg/mL (312 mmol/L) fleshly $NaBH_4$ was rapidly added, and the solution was stirred continuously for 30 min. The solution turned from faint yellow to reddish-brown. The methanol was removed under reduced pressure at 50 °C, and 5.0 mL of ultrapure water was added into the residue. The concentration of AgNPs@PDMAEMA-C_4 was 129 μg/mL (Ag mass concentration).

Fluorescence Polarization Measurement. The fast-growing *Pseudomonas aeruginosa* and *Staphylococcus aureus* (5.0×10^7 CFU/mL) were washed twice with PBS and resuspended in 1.0 mL of PBS. The bacteria were treated with AgNPs@PDMAEMA-C_4 of a series of concentration for 20 min. Then 1.0 mL of 1.0×10^{-5} mol/L fluorescent membrane probe, 1,6-diphenyl-1,3,5-hexatriene (DPH, Molecular Probes, Aladdin), was added to each treated bacteria and incubated in the dark for 15 min to allow the probe incorporation into the cytoplasmic membrane. Finally, the bacterial cells were rinsed with PBS and resuspended in 1.0 mL of PBS for the fluorescence measurements.

The steady-state fluorescence measurements were performed with a Shimadzu RF-5301PC spectrofluorometer using 1 cm path length quartz cuvettes. Excitation and emission wavelengths were set at 360 and 442 nm, respectively. Polarizers were set in either a vertical or horizontal position. The slit widths for the excitation and emission beams were both 5 nm. Background intensities of samples were subtracted from each sample spectrum to cancel out any contribution due to the solvent Raman peak and other scattering artifacts. Fluorescence polarization measurement was performed using a Shimadzu polarization accessory. Polarization values were calculated from the following equation:[7]

$$\text{polarization values} = \frac{I_{VV} - GI_{VH}}{I_{VV} + GI_{VH}}$$

$$G = \frac{I_{HV}}{I_{HH}}$$

where I_{VV} was the fluorescence intensity with vertical excitation and vertical emission, I_{VH} was the fluorescence intensity with vertical excitation and horizontal emission, I_{HV} was the fluorescence intensity with horizontal excitation and vertical emission, and I_{HH} was the fluorescence intensity with horizontal excitation and horizontal emission. The correlation factor G was defined as the ratio of I_{HV} to I_{HH}.

Inhibition of Enzyme β-galactosidase Activity. The *Escherichia coli* suspension (40 mL, about 5.0×10^8 CFU/mL) was harvested by centrifuging (5000 rpm) at 4 °C for 5 min and washing with PBS three times. The supernatant was discarded, and the remaining bacteria were resuspended in 15 mL of PBS. The solution containing the cytoplasm was extracted from the bacteria by ultrasound for 12 h in an ice−water bath and filtrated through a 0.22 μm cellulose membrane. Then, 0.5 mL of AgNPs@PDMAEMA-C_4 (0.6, 1.5, and 3.0 μg/mL), AgNPs (0.6 μg/mL) suspensions, and ultrapure water were added to 1.0 mL of the filtrate. After incubation for 30 min, 1.0 mL of 10 mg/mL ortho-nitrophenyl-β-D-galactopyranoside (ONPG) was added. The generated ortho-nitrophenol (ONP) was determined by monitoring the optical density at 420 nm (OD_{420}) using UV−vis spectroscopy. The control assay was carried out by the addition of ultrapure water. The percentage of β-galactosidase inhibition was calculated as follows:

$$\%\ \text{inhibition} = \frac{OD_{420}(\text{control}) - OD_{420}(\text{sample})}{OD_{420}(\text{control})} \times 100\%$$

Preparation of Ultrathin Sections of Bacterial Samples for TEM. The bacterial suspensions (1.0×10^8 CFU/mL) of *P. aeruginosa* and *S. aureus* were washed twice with PBS and resuspended in 1.5 mL of PBS. The samples were subsequently incubated for 30 min at 37 °C with 100 μL of 32 μg/mL AgNPs@PDMAEMA-C_4 solution. Free AgNPs@PDMAEMA-C_4 was removed by centrifuging (5000 rpm) at 4 °C for 5 min and washing with PBS three times. The remaining bacteria were fixed with 1.0 mL of 2.5% glutaraldehyde in cacodylate buffer (0.1 mol/L, pH 7.4) for 4 h. The treated bacterial samples were washed twice with PBS and further fixed with 200 μL of 1.5% osmic acid for 2 h. The obtained residues were washed thrice with PBS, dehydrated using graded ethanol solutions (30, 50, 70, 90, 95, and 100%, v/v in water) and 50% acetone (v/v, in ethanol) for 15 min, and finally dehydrated twice with pure acetone for 15 min. Then, the dehydrated samples were embedded in graded QUETOL 651 resin solutions (1:3, 1:1, and 3:1 v/v in acetone) and pure resin containing DMP-30 overnight and polymerized at 60 °C for 24 h. Subsequently, ultrathin sections of about 60 nm were cut with a Leica EM UC6 ultramicrotome and placed on a carbon-coated copper grid. The slices were stained with 2% uranyl acetate and 0.2% lead citrate before observation. Digital images were acquired using a TEM with an OSIS MEGAVIEW G2 CCD Digital Camera system.

Induction of Bacterial Resistance. An overnight culture of *P. aeruginosa* and *S. aureus* was inoculated into the Luria-Bertani (LB) broth containing 1/2 minimum inhibitory concentration (MIC) of AgNPs@PDMAEMA-C_4 or levofloxacin, respectively. The bacteria were incubated at 37 °C until a concentration of 2.0×10^7 colony forming units per milliliter (CFU/mL) was reached. These bacterial cells were inoculated on agar plates containing the nanoparticles or levofloxacin, and susceptibility to the nanoparticles or levofloxacin was examined by MIC assay. To obtain resistant variants, we passaged the cultures 30 times in the presence of increasing concentrations of the nanoparticles or levofloxacin based on the growth conditions of the variants, and the MIC was determined after each passage.

In Vivo Studies. The studies were prepared by following our previously published article.[8] Different from the previous procedure, four wounds were made on the left and right side of the backbone of each rat. A diagrammatic sketch of the four wounds with different treatments can be seen in Figure S1 (Supporting Information). The detailed experimental description has already been provided in Supporting Information.

RESULTS AND DISCUSSION

Synthesis of AgNPs@PDMAEMA-C_n. In this work, we synthesized a multivalent antimicrobial nanoparticle by facile reduction of $AgNO_3$ with $NaBH_4$ in the presence of a cationic polymer (PDMAEMA-C_n) via the "grafting to" approach (Figure 1). The cationic polymer was prepared by RAFT polymerization of DMAEMA, in which thiocarbonylthio compounds act as chain transfer agents to bear dithioester end groups. The PDMAEMA chains were quaternized with alkyl bromide in the tertiary amino groups and subsequently used as templates to prepare cationic polymer-functionalized AgNPs. Upon the addition of $AgNO_3$ to the PDMAEMA-C_n solution, silver ions were easily adsorbed into the core of polymer micelles via complexation reaction with dithioester

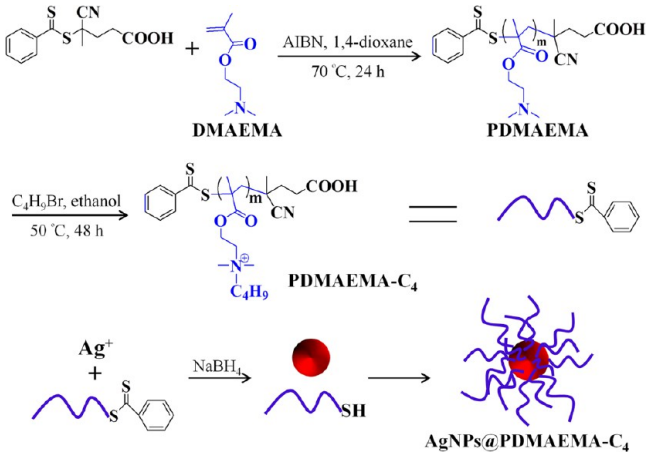

Figure 1. Schematic representation of the synthesis of AgNPs@PDMAEMA-C_4.

groups. The simultaneous reduction of dithioester end groups to thiols in the presence of silver ions led to the generation of AgNPs@PDMAEMA-C_n.

Optimization of Synthesis Conditions of AgNPs@PDMAEMA-C_n. The membrane-disrupting activity of cationic polymers is reported to be mainly dependent on the length of the alkyl tail, which also influences the balance between the antimicrobial and cytotoxic properties of these polymers.[9] Therefore, PDMAEMA quaternization with different alkyl bromide would affect antibacterial activity and cytotoxicity of the nanoparticles. To assess their effects, PDMAEMA was quaternized with 1-bromoethane (C_2), 1-bromobutane (C_4), 1-bromooctane (C_8), 1-bromododecane (C_{12}), and 1-bromohexadecane (C_{16}), respectively, and then reacted with silver ions to form the nanoparticles. The quaternization degree of PDMAEMA was 82.2, 81.3, 80.3, 67.5, and 55.3, respectively. The MIC assay confirmed that the antibacterial activity against *P. aeruginosa* and *S. aureus* was greater when the PDMAEMA was quaternized with C_2, C_4, and C_8 rather than with C_{12} and C_{16} (Figure 2A). It was possibly because a longer alkyl chain induced a greater hydrophobicity, leading to the decrease of antibacterial activity. The cell viability of the nanoparticles with different alkyl chains and different concentrations (1.0 and 2.0 μg/mL) were used to evaluate the cytotoxic effect against NIH3T3 cell (Figure 2B,C). The cell viability of PDMAEMA quaternization with C_2 and C_4 was clearly higher than that of the PDMAEMA quaternized with a longer alkyl chain and maintained over 80%. Taken together, the optimal alkyl bromide was C_4.

To investigate the effect of molar ratio of PDMAEMA-C_4 to silver on antibacterial activity, AgNPs@PDMAEMA-C_4 with different molar ratios (total molar maintained constant) were synthesized and characterized with UV−vis spectrum, size, and Zeta potential (Figure 2D,E). As the molar ratio of PDMAEMA-C_4 to silver increased, the UV−vis absorption intensity decreased, the plasmon absorption red-shifted, the size decreased, and the Zeta potential increased. MIC value against *P. aeruginosa* and *S. aureus* was determined to evaluate the antibacterial activity of the nanoparticles with different molar ratios, and the results are shown in Figure 2F. The higher ratio of PDMAEMA-C_4 was able to offer a lower MIC value. However, further increase of the ratio of PDMAEMA-C_4 would cause a high MIC value. Generally, the nanoparticles with lower MIC values are considered more effective antimicrobial materials. Therefore, a 1:1 molar ratio of PDMAEMA-C_4 to silver was employed.

To examine the effect of $NaBH_4$ volume on antibacterial activity, we synthesized the nanoparticles with $NaBH_4$ volume from 50 to 300 μL and characterized them by UV−vis spectrum, size, and Zeta potential (Figure 2G,H). With the increase of $NaBH_4$ volume, the UV−vis absorption intensity increased, the absorption spectra blue-shifted, and the size and Zeta potential decreased. The antibacterial activity of the nanoparticles with different $NaBH_4$ volumes was studied by MIC value against *P. aeruginosa* and *S. aureus*. As shown in Figure 2I, MIC value decreased with increasing $NaBH_4$ volume and reached a minimum of 150 μL. Therefore, 150 μL of $NaBH_4$ was chosen.

The effect of molecular weight of PDMAEMA-C_4 on antibacterial activity was also studied. The nanoparticles with different molecular weights of PDMAEMA-C_4 were synthesized and characterized with UV−vis spectra and gel permeation chromatography (GPC; Figure 2J,K and Table S1, Supporting Information). The GPC traces of homogeneous polymer PDMAEMA were monomodal and had a reasonably narrow molecular weight distribution (polydispersity index (PDI) < 1.25). The quaternization degree of PDMAEMA-C_4 with different molecular weights was in the range of 72.2−81.3%. Moreover, the UV−vis absorption intensity decreased as the molecular weight increased. The antibacterial activity of the nanoparticles with PDMAEMA-C_4 of different molecular weights was estimated by MIC value against *P. aeruginosa* and *S. aureus*, respectively. The results showed that the MIC value increased with increasing molecular weight (Figure 2L). Therefore, the molecular weight of 8427 Da was selected.

Characterization of AgNPs@PDMAEMA-C_4. The formation of AgNPs@PDMAEMA-C_4 was observed under TEM. There are differences between the TEM images of AgNPs and AgNPs@PDMAEMA-C_4 (Figure 3A,B). When compared with AgNPs, the appearance of the polymer corona has been formed around the nanoparticles. From a pictorial representation (Figure 3C), it is clear that the color of nanoparticle solution changed from yellow to reddish-brown as the PDMAEMA-C was fixed on AgNPs, indicating the formation of AgNPs@PDMAEMA-C_4. UV−vis absorption spectra of AgNPs and AgNPs@PDMAEMA-C_4 are shown in Figure 3D. The maximum absorption of nanoparticles showed a red shift from 396 to 444 nm when compared with that of AgNPs. Moreover, low peak intensity and increased peak width appeared when compared with those of the uncapped AgNPs. These results were possibly caused by a loss of the surface plasmon resonance absorbance of AgNPs.

Antibacterial Activity of AgNPs@PDMAEMA-C_4. The antibacterial activity of AgNPs@PDMAEMA-C_4 was evaluated by growth inhibition of *P. aeruginosa* and *S. aureus* in the presence of the nanoparticle with different concentrations and determination their the optical density at 600 nm (OD_{600}) after 12 h. As shown in Figure S7 (Supporting Information), the growth of *P. aeruginosa* and *S. aureus* was inhibited, while the concentration of nanoparticles was more than 0.4 and 0.2 μg/mL, respectively. The cationic polymers (e.g., PDMAEMA-C_4) do not have a specific target toward the bacteria, and they interact with bacterial membranes based on electrostatic interaction. We believe that the high local density of positive charges on the nanoparticles leads to stronger electrostatic interaction with the bacterial membranes and subsequently efficiently kills the bacteria.

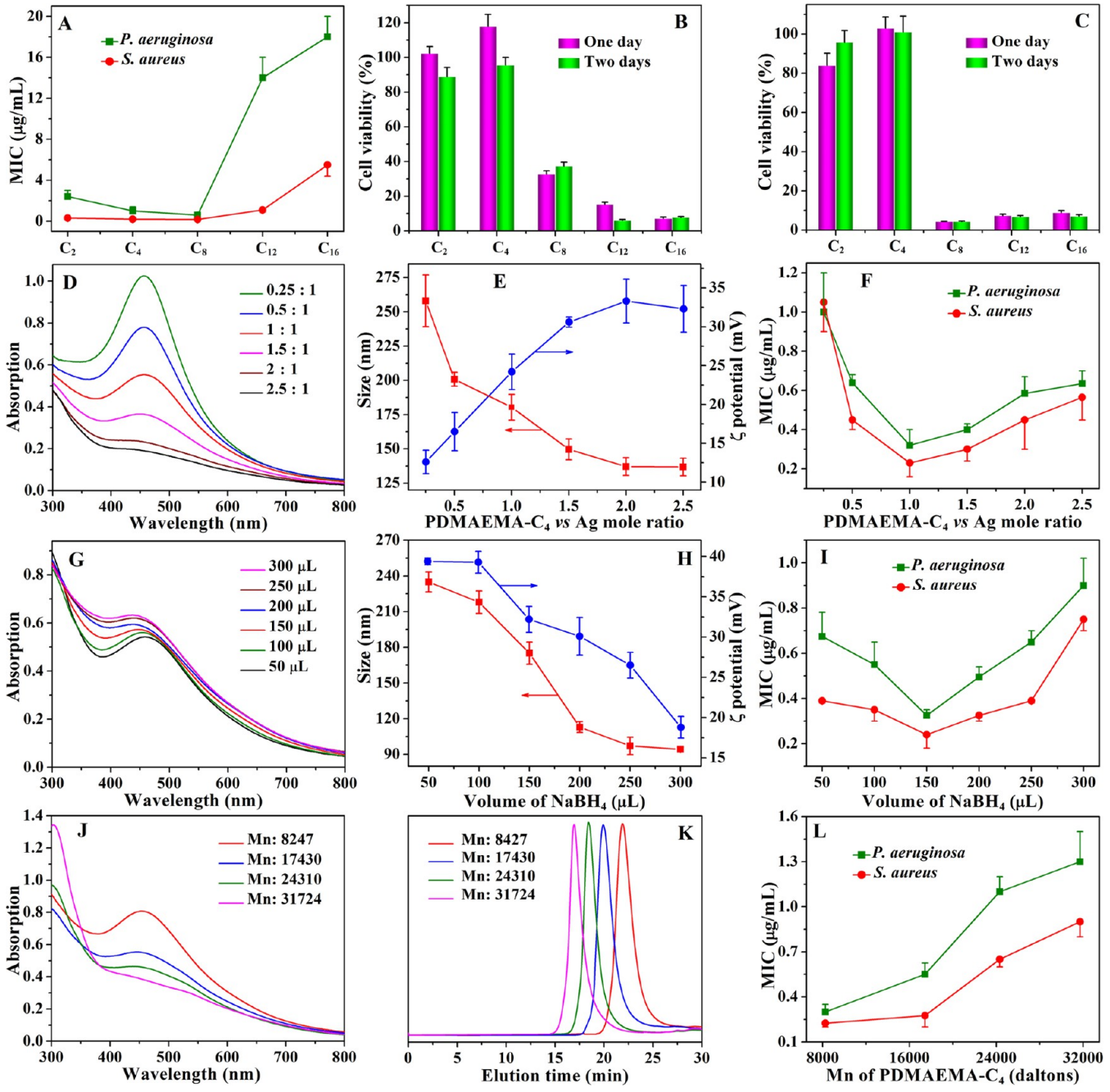

Figure 2. Optimization of synthesis conditions of AgNPs@PDMAEMA-C_4. (A) The effect of a different alkyl chain on MIC value; (B and C) the effect of a different alkyl chain on the cytotoxicity effect of the nanoparticles with different concentrations (B and C are 1.0 and 2.0 μg/mL, respectively) against NIH3T3 cells; the effects of molar ratio of PDMAEMA-C_4 and silver on (D) UV−vis spectrum, (E) size, Zeta potential, and (F) MIC value; the effects of volume of reducing agent on (G) UV−vis spectrum, (H) size, Zeta potential, and (I) MIC value; the effects of molecular weight of PDMAEMA-C_4 on (J) UV−vis spectrum and (L) MIC value; and (K) the GPC traces of PDMAEMA with different molecular weight.

To confirm the polyvalent and synergistic effects between AgNPs and PDMAEMA-C_4, we tested the zone of inhibition. For this purpose, 12.84 mg/mL PDMAEMA-C_4 (214 μL of 300 mg/mL PDMAEMA-C_4 diluted in 5.0 mL), 129 μg/mL AuNPs@PDMAEMA-C_4 (PDMAEMA-C_4-stabilized gold nanoparticles using the same synthetic method as AgNPs@PDMAEMA-C_4), 129 μg/mL AgNPs (about 5.0 nm in size), and 129 μg/mL AgNPs@PDMAEMA-C_4 were prepared. As shown in Figure 4, the diameters of the zones of inhibition of AuNPs@PDMAEMA-C_4 were larger than those of PDMAEMA-C_4. In general, larger diameters of the bacteria-free zone surrounding the disk signify that bacteria are more sensitive to the antimicrobial materials contained in the disk. Due to weak antibacterial activity, AuNPs are often used as molecular scaffolds for obtaining bound molecules in multiple copies, which may facilitate the polyvalent effects of polymers.[10] Moreover, the diameters of the zones of inhibition of AgNPs@PDMAEMA-C_4 were significantly larger than those of PDMAEMA-C_4 and AgNP alone, which is suggestive of excellent synergistic activity between AgNPs and PDMAE-

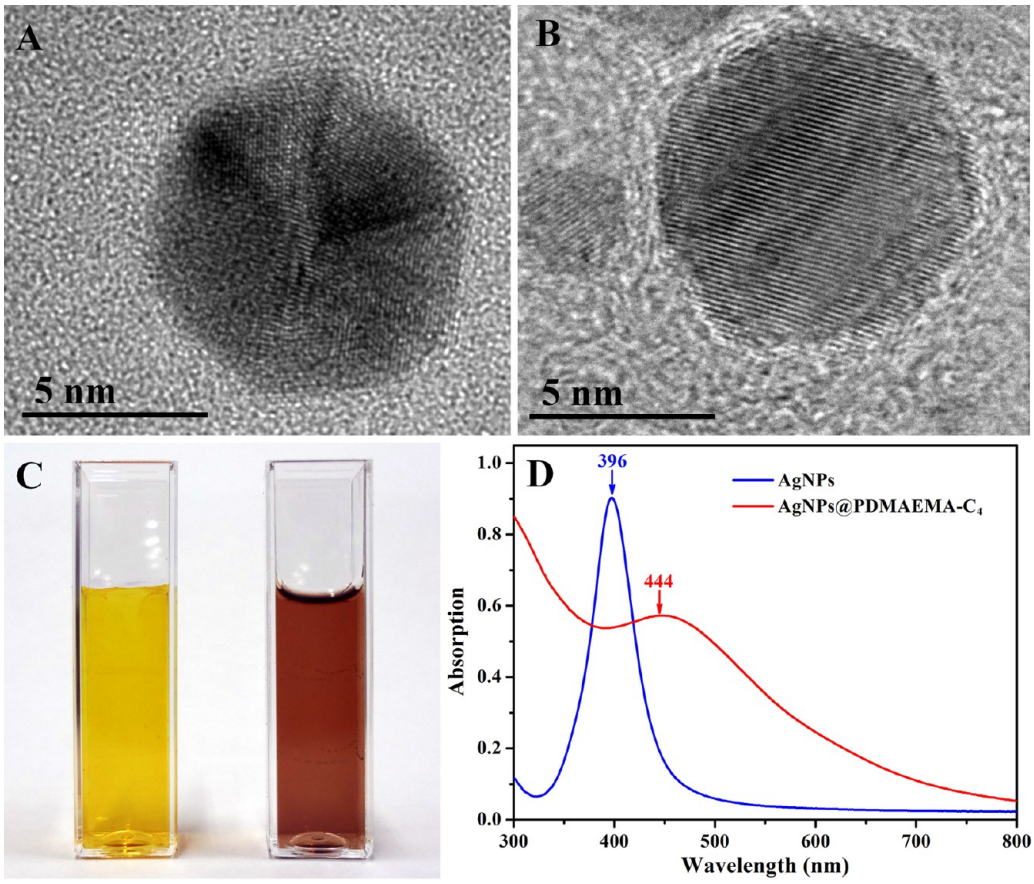

Figure 3. Characterization of AgNPs@PDMAEMA-C_4. TEM images of (A) AgNPs and (B) AgNPs@PDMAEMA-C_4; (C) a photograph of (left) AgNPs and (right) AgNPs@PDMAEMA-C_4; and (D) UV−vis spectra of AgNPs and AgNPs@PDMAEMA-C_4.

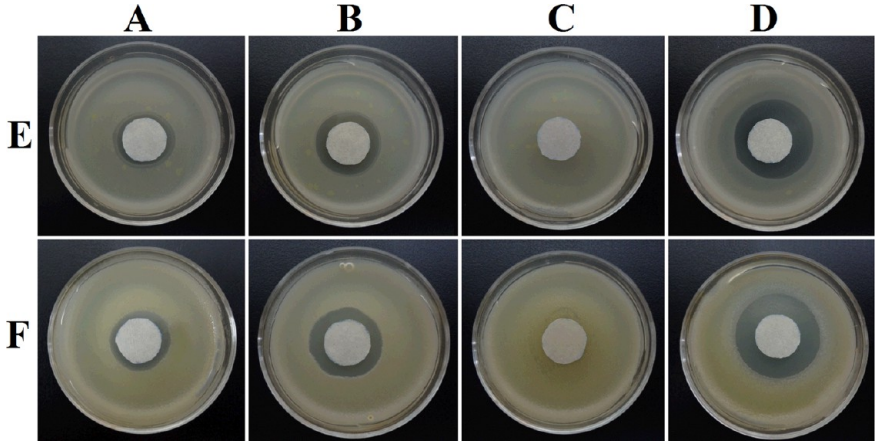

Figure 4. Inhibition zones of (A) PDMAEMA-C_4, (B) AuNPs@PDMAEMA-C_4, (C) AgNPs, and (D) AgNPs@PDMAEMA-C_4 against (E) *P. aeruginosa* and (F) *S. aureus*.

MA-C_4. Clearly, AgNPs@PDMAEMA-C_4 exerts polyvalent and synergistic antibacterial effects, leading to superior antibacterial performance against both Gram-negative and Gram-positive bacteria.

The LIVE/DEAD bacterial cell viability assay was used to further confirm the antibacterial activity of AgNPs@PDMAEMA-C_4. Under the fluorescence microscope, the living/dead bacterial cells appeared as green/red points with intact/damaged cell membranes. Fluorescence micrographs of *P. aeruginosa* and *S. aureus* before and after treatment with AgNPs@PDMAEMA-C_4 for 0 and 20 min are shown in Figure 5. The untreated bacterial cells exhibited green fluorescence, indicating that they were alive (Figure 5A,C). After treatment with AgNPs@PDMAEMA-C_4 for 20 min, the red fluorescence was observed, suggesting that the bacteria were dead (Figure 5B,D). Therefore, the result confirmed that the nanoparticles can rapidly and efficiently kill the bacteria.

Antibacterial Mechanism of AgNPs@PDMAEMA-C_4. To assess the mechanism underlying the antibacterial action of AgNPs@PDMAEMA-C_4, we performed fluorescence polarization of DPH, which offers a means of quantitatively measuring the relative changes in fluidity of the bacterial

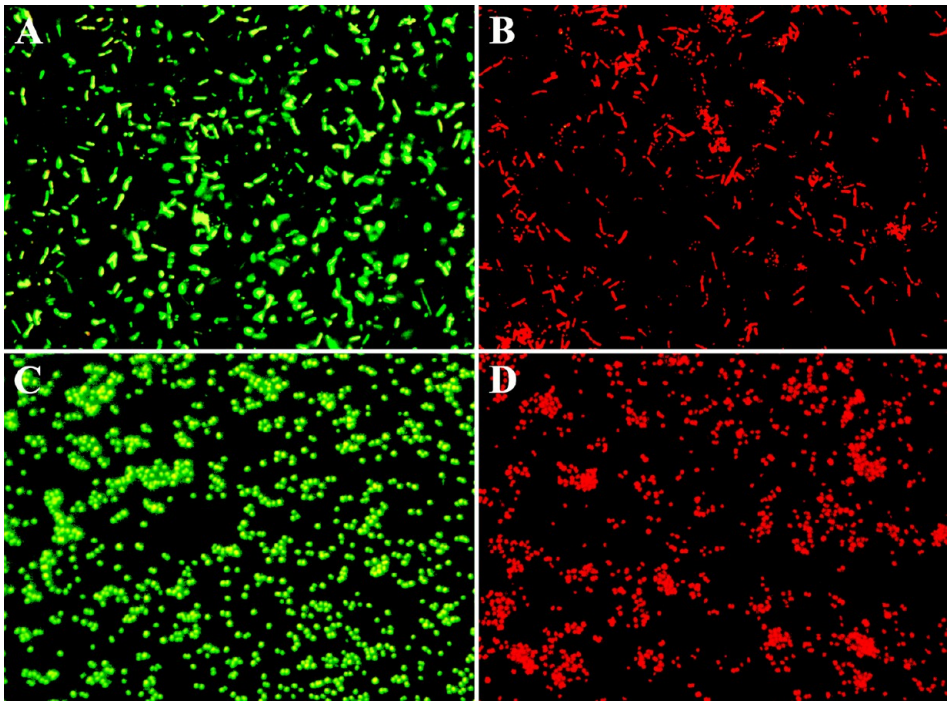

Figure 5. Fluorescence micrograph of (A and B) *P. aeruginosa* and (C and D) *S. aureus* after being treated with AgNPs@PDMAEMA-C_4 for (A and C) 0 and (B and D) 20 min.

cytoplasmic membrane under different growth conditions.[11] The DPH fluorescent probe is hydrophobic and easily associates with lipophilic tails of phospholipids in the cytoplasmic membrane without disrupting their structure.[12] Membrane polarization values were estimated as the averages of total cells, whereby a small change reflects significant alterations in the membrane structure. A high polarization value indicates low membrane fluidity.[13] Polarization values as a function of concentration alterations of nanoparticles are shown in Figure 6. Bacterial cells grown in the absence of nanoparticles exhibited lower values than those grown in the presence of nanoparticles. Moreover, polarization values increased with increasing nanoparticle concentrations in both *P. aeruginosa* and *S. aureus*. Positively charged nanoparticles can bind to the negatively charged cell surface of bacteria via electrostatic interactions. The alkyl chain of external PDMAEMA-C_4 of nanoparticles provides a lipophilic segment compatible with the lipid bilayer of the bacterial cytoplasmic membrane.[14] This nanoparticle hinders bacterial modulation of membrane composition to maintain fluidity for cell growth and division, leading to a decrease in fluidity and disruption of the bacterial cytoplasmic membrane.[15] Eventually, nanoparticles penetrate through the bacterial membrane to further affect intracellular function. Therefore, the obvious changes in polarization following a concentration shift of nanoparticles correspond closely with the concentration-dependent alterations in growth inhibition of bacterial cells, suggesting that decrease in membrane fluidity is one of the main causes of bacterial death.

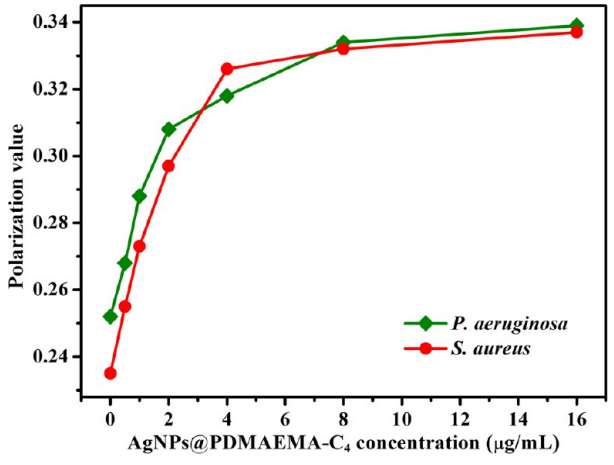

Figure 6. Change of membrane polarization values for *P. aeruginosa* and *S. aureus* previously grown in the presence of AgNPs@ PDMAEMA-C_4 with different concentrations.

Following the disruption of the bacterial cytoplasmic membrane, AgNPs@PDMAEMA-C_4 can penetrate the cytoplasm. To investigate whether the nanoparticles disrupt the activity of vital intracellular substances, β-galactosidase present in the cytoplasm of *E. coli* was used as the research object model. β-Galactosidase catalyzes the hydrolysis of ONPG to release ONP, measured at OD_{420} using UV−vis spectroscopy.[16] However, if β-galactosidase activity is inhibited by nanoparticles, ONP generation is decreased. In the present study, 34.2, 41.5, and 50.7% inhibition of β-galactosidase activity was observed with 0.6, 1.5, and 3.0 μg/mL AgNPs@PDMAEMA-C_4, respectively. Meanwhile, inhibition by 0.6 μg/mL AgNPs was 55.6%. Clearly, activity was decreased with increasing concentrations of AgNPs@PDMAEMA-C_4. Moreover, inhibition by AgNPs was stronger than that by AgNPs@ PDMAEMA-C_4 at the same concentrations, suggesting that AgNP within the nanocomposite plays a major role in the inhibition of β-galactosidase activity, rather than surface PDMAEMA-C_4. With regard to the mechanism underlying the inhibition of enzymatic and protein activity, it is possible that AgNPs interact strongly with the thiol groups of intracellular enzymes and proteins, leading to degeneration.[17]

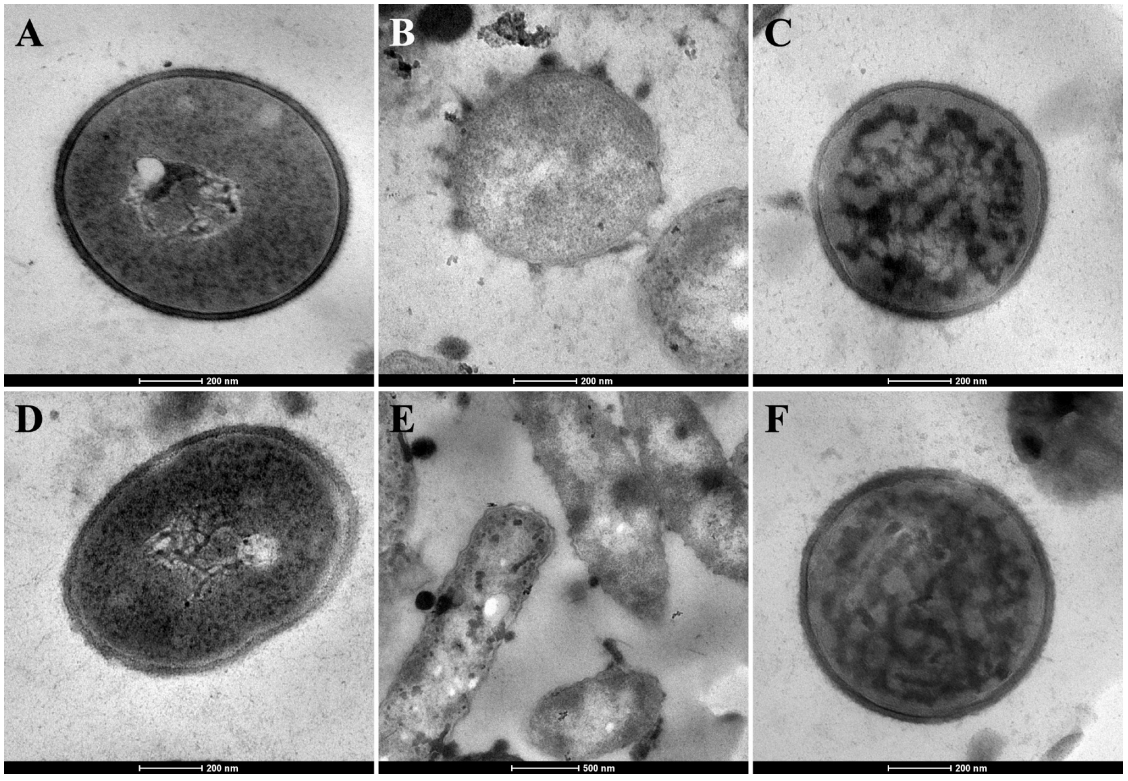

Figure 7. TEM images of a thin section of (A−C) *S. aureus* and (D−F) *P. aeruginosa* (A and D) before and (B, C, E, and F) after incubation with AgNPs@PDMAEMA-C_4 for 30 min.

Generally, the enzymatic and protein activities were the close relation to their physiological functions.[18] Therefore, it can be concluded that AgNPs@PDMAEMA-C_4 could affect the physiological functions of intracellular enzymes and proteins, leading to inhibition of activity and cellular damage.

To further clarify the essential antibacterial mechanism of the action of nanoparticles, we investigated ultrastructural damage of *S. aureus* and *P. aeruginosa* before and after incubation with nanoparticles through examination of TEM images of ultrathin sections. Untreated bacteria exhibited a smooth surface and distinct nucleoid structures (Figure 7A,D). In contrast, the bacterial cell surface became rough after incubation with nanoparticles at a concentration of 2.0 μg/mL for 30 min. Moreover, numerous blebs formed with cytoplasmic release (Figure 7B,E). Bleb formation on the bacterial surface has been observed when bacteria are treated with cationic polymers, peptides, and antibiotics.[19−21] The penetration of positively charged nanoparticles into negatively charged bacterial cytomembranes via electrostatic interactions accelerates cell division, leading to the formation of blebs. In addition, the alkyl chain of the nanoparticle surface can decrease membrane fluidity and disrupt the cytoplasmic membrane. These two factors act together to damage the bacterial cytomembrane, resulting in leakage of intracellular content. As shown in Figure 7C,F, floccules were observed within bacteria, leading to intracellular chaos. It is possible that the nanoparticles react with the intracellular enzymes, and proteins and inhibit their activity. Therefore, positively charged nanoparticles increase the permeability of the cytoplasmic bacterial membrane due to the presence of external PDMAEMA-C_4. Subsequently, these nanoparticles penetrate the cells and strongly associate with intracellular enzymes and proteins, resulting in cell death.

Bacterial Resistance by AgNPs@PDMAEMA-C_4. To investigate potential bacterial resistance against AgNPs@PDMAEMA-C_4, we induced nanoparticle and levofloxacin resistance in cultures of *P. aeruginosa* and *S. aureus*, respectively. After 30 passages, the MIC value of nanoparticles against *P. aeruginosa* and *S. aureus* remained constant compared to the original value, indicating no emerging bacterial resistance. However, the MIC of levofloxacin increased from 3.2 to 156 μg/mL against *P. aeruginosa* and from 0.64 to 78 μg/mL against *S. aureus* during the 30 passages, illustrating emergence of bacterial resistance to the drug. We conclude that synthetic AgNPs@PDMAEMA-C_4 with a double mechanism of antibacterial action, as well as disruption of membrane structure and inhibition of enzymatic activity, is able to efficiently suppress the emergence of bacterial resistance. Moreover, convergence of multiple antimicrobial components in a single material does not induce bacterial resistance.[22]

Cell Viability. The cytotoxicity of nanoparticles against NIH3T3 cells was evaluated using the MTT assay. The cell viability of nanoparticles as a function of concentration (from 0.5 to 8.0 μg/mL) and incubation time is presented in Figure S8 (Supporting Information). Cell viability of nanoparticles was over 80% at concentrations ≤8.0 μg/mL, which exceeded MIC of nanoparticles against *P. aeruginosa* and *S. aureus* by 20-fold. Thus, nanoparticles have potential for wound treatment owing to good cytocompatibility and efficient antibacterial activity.

In Vivo Study. To assess the wound healing status and effects on dermal tissue of healthy and diabetic rats after administration of AgNPs@PDMAEMA-C_4, we photographed the wounds on the rats on days 1, 8, 12, 18, and 24, and we performed histological evaluation of the rat dermal wounds on day 24 after treatment. Data from the representative wound photographs of diabetic rats (Figure 8A−E) revealed that the

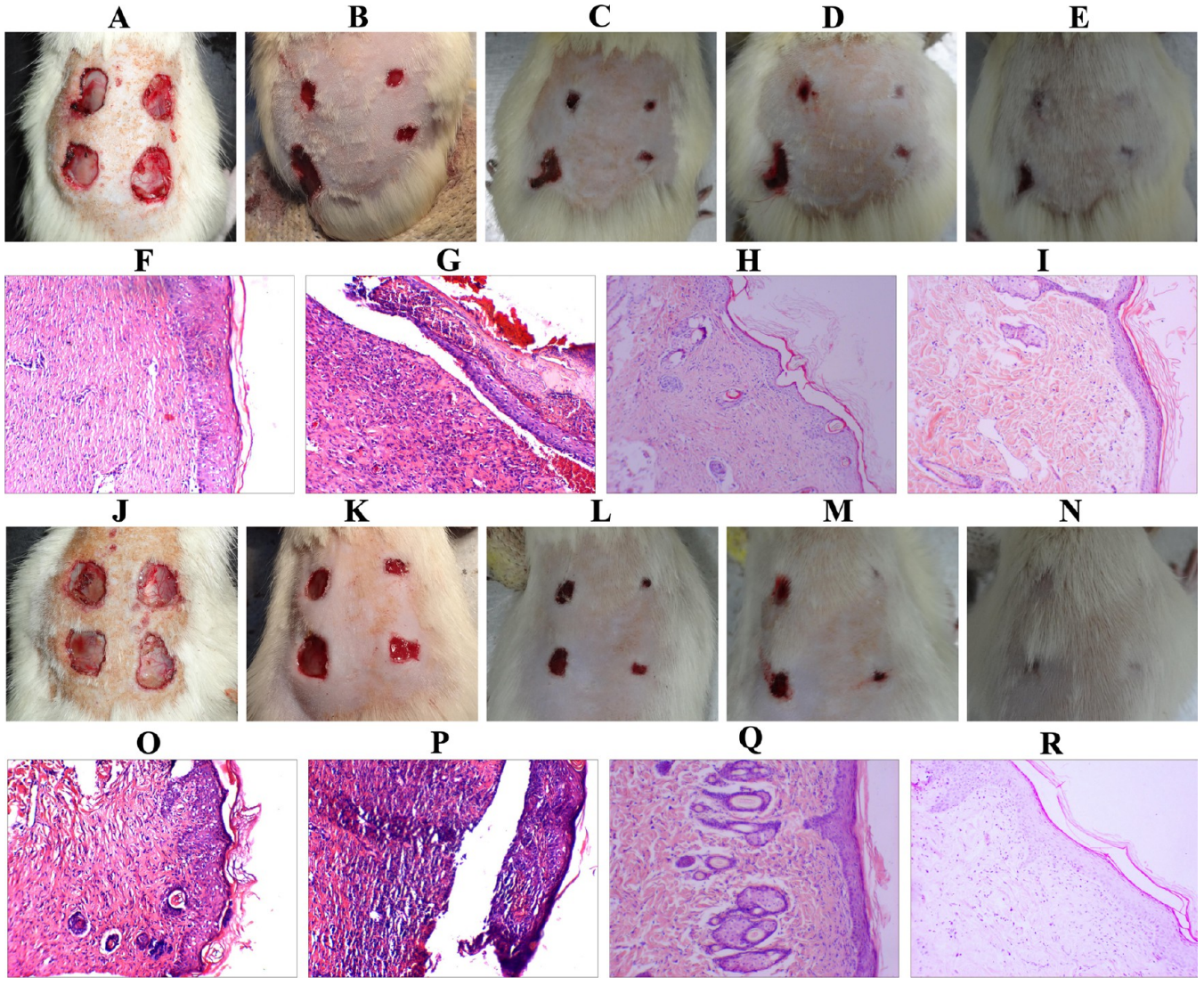

Figure 8. In vivo study on the effects of treatment of *P. aeruginosa* and *S. aureus*-induced wound infections for (A–I) diabetic and (J–R) healthy rats with AgNPs@PDMAEMA-C_4 (n = 7). Wound photographs of the rats taken on days (A and J) 1, (B and K) 8, (C and L) 12, (D and M) 18, and (E and N) 24; H&E staining of the rat dermal wound of the (F and O) treatment, (G and P) model, (H and Q) drug control, and (I and R) blank control groups after 24 days.

wounds of the treatment group healed after 24 days, similar to that of the drug control and blank control groups. However, wounds of the model group visibly deteriorated with lower rates of healing owing to their damaged immune systems. As shown in the photographs of healthy rats (Figure 8J–N), wounds of the treatment group healed after 24 days and showed faster healing than the model group. From representative hematoxylin and eosin (H&E)-stained histological images of diabetic (Figure 8F–I) and healthy (Figure 8O–R) rats, epithelialization, formation of granulation tissue, and contraction of underlying wound connective tissues were observed, which are indicative of wound healing. However, as shown in Figure 8 (G,P), the wounds did not heal, and massive inflammatory cells were observed at the wound site due to infection without perfect repair in the model group. Therefore, AgNPs@PDMAEMA-C_4 not only had no effect on dermal tissue but also promoted wound healing, especially in bodies with damaged immune systems.

CONCLUSIONS

In conclusion, we have successfully synthesized an effective antimicrobial nanoparticle by covalent attachment of thiol end-capped PDMAEMA-C_4 to AgNPs. Owing to the polyvalent and synergistic antibacterial functions of these nanoparticles, antimicrobial activity was strongly enhanced with no bacterial resistance. The novel nanoparticle increased bacterial cytoplasmic membrane permeability, causing membrane disruption, and subsequently penetrated cells and strongly inhibited intracellular enzyme activity, leading to cell death. Moreover, our nanoparticle promoted healing after *P. aeruginosa*- and *S. aureus*-induced infection. Notably, the same curative effect was observed in a diabetic rat model, indicating that AgNPs@PDMAEMA-C_4 acts as an efficient antimicrobial material with potential for treating bacteria-induced infections in patients with low immunity.

■ ASSOCIATED CONTENT

Supporting Information

Materials, synthesis of PDMAEMA, quaternization of PDMAEMA, characterization, minimal inhibitory concentration, zone of inhibition test, fluorescence microscopic observation, cytotoxicity assay, in vivo studies, study of the stability, ^{1}H NMR, FTIR, Zeta potentials, and XRD. This material is available free of charge via the Internet at http://pubs.acs.org.

■ AUTHOR INFORMATION

Corresponding Authors

*Tel.: +86 22 23501645. Fax: +86 22 23505598. E-mail: zhangxinge@nankai.edu.cn.
*E-mail: lcx@nankai.edu.cn.

Notes

The authors declare no competing financial interest.

■ ACKNOWLEDGMENTS

This work was supported by the National Natural Science Foundation of China (Grant No. 21174071) and the Program for Changjiang Scholars and Innovative Research Team in University (IRT 1257).

■ REFERENCES

(1) *Antibiotic Resistance Threats in the United States, 2013*. Department of Health and Human Services, Centers for Disease Control and Prevention, U.S. Government Printing Office: Washington, DC, 2013.
(2) Murata, H.; Koepsel, R. R.; Matyjaszewski, K.; Russell, A. J. Permanent, Non-Leaching Antibacterial Surface—2: How High Density Cationic Surfaces Kill Bacterial Cells. *Biomaterials* **2007**, *28*, 4870−4879.
(3) Cado, G.; Aslam, R.; Séon, L.; Garnier, T.; Fabre, R.; Parat, A.; Chassepot, A.; Voegel, J. C.; Senger, B.; Schneider, F.; Frère, Y.; Jierry, L.; Schaaf, P.; Kerdjoudj, H.; Metz-Boutigue, M.-H.; Boulmedais, F. Self-Defensive Biomaterial Coating against Bacteria and Yeasts: Polysaccharide Multilayer Film with Embedded Antimicrobial Peptide. *Adv. Funct. Mater.* **2013**, *23*, 4801−4809.
(4) Li, Y.; Fukushima, K.; Coady, D. J.; Engler, A. C.; Liu, S.; Huang, Y.; Cho, J. S.; Guo, Y.; Miller, L. S.; Tan, J. P.; Ee, P. L.; Fan, W.; Yang, Y. Y.; Hedrick, J. L. Broad-Spectrum Antimicrobial and Biofilm-Disrupting Hydrogels: Stereocomplex-Driven Supramolecular Assemblies. *Angew. Chem., Int. Ed. Engl.* **2013**, *52*, 674−678.
(5) Bagheri, M.; Beyermann, M.; Dathe, M. Immobilization Reduces the Activity of Surface-Bound Cationic Antimicrobial Peptides with No Influence Upon the Activity Spectrum. *Antimicrob. Agents Chemother.* **2009**, *53*, 1132−1141.
(6) Chen, X.; Schluesener, H. J. Nanosilver: A Nanoproduct in Medical Application. *Toxicol. Lett.* **2008**, *176*, 1−12.
(7) Chen, R. F.; Bowman, R. L. Fluorescence Polarization: Measurement with Ultraviolet-Polarizing Filters in a Spectrophotofluorometer. *Science* **1965**, *147*, 729−732.
(8) Mei, L.; Lu, Z. T.; Zhang, W.; Wu, Z. M.; Zhang, X. G.; Wang, Y. N.; Luo, Y. T.; Li, C. X.; Jia, Y. X. Bioconjugated Nanoparticles for Attachment and Penetration into Pathogenic Bacteria. *Biomaterials* **2013**, *34*, 10328−10337.
(9) Tew, G. N.; Liu, D.; Chen, B.; Doerksen, R. J.; Kaplan, J.; Carroll, P. J.; Klein, M. L.; DeGrado, W. F. De Novo Design of Biomimetic Antimicrobial Polymers. *Proc. Natl. Acad. Sci. U.S.A.* **2002**, *99*, 5110−5114.
(10) Gu, H. W.; Ho, P. L.; Tong, E.; Wang, L.; Xu, B. Presenting Vancomycin on Nanoparticles to Enhance Antimicrobial Activities. *Nano Lett.* **2003**, *3*, 1261−1263.
(11) Mykytczuk, N. C. S.; Trevors, J. T.; Leduc, L. G.; Ferroni, G. D. Fluorescence Polarization in Studies of Bacterial Cytoplasmic Membrane Fluidity under Environmental Stress. *Prog. Biophys. Mol. Biol.* **2007**, *95*, 60−82.
(12) Vincent, M.; England, L. S.; Trevors, J. T. Cytoplasmic Membrane Polarization in Gram-Positive and Gram-Negative Bacteria Grown in the Absence and Presence of Tetracycline. *Biochim. Biophys. Acta* **2004**, *1672*, 131−134.
(13) Trevors, J. T. Fluorescent Probes for Bacterial Cytoplasmic Membrane Research. *J. Biochem. Biophys. Methods* **2003**, *57*, 87−103.
(14) Goodson, B.; Ehrhardt, A.; Ng, S.; Nuss, J.; Johnson, K.; Giedlin, M.; Yamamoto, R.; Moos, W. H.; Krebber, A.; Ladner, M.; Giacona, M. B.; Vitt, C.; Winter, J. Characterization of Novel Antimicrobial Peptoids. *Antimicrob. Agents Chemother.* **1999**, *43*, 1429−1434.
(15) Beney, L.; Gervais, P. Influence of the Fluidity of the Membrane on the Response of Microorganisms to Environmental Stresses. *Appl. Microbiol. Biotechnol.* **2001**, *57*, 34−42.
(16) Vestro, L. S.; Weiser, J. N.; Axelsen, P. H. Antibacterial and Antimembrane Activities of Cecropin A in *Escherichia coli*. *Antimicrob. Agents Chemother.* **2000**, *44*, 602−607.
(17) Alt, V.; Bechert, T.; Steinrücke, P.; Wagener, M.; Seidel, P.; Dingeldein, E.; Domann, E.; Schnettler, R. An in Vitro Assessment of the Antibacterial Properties and Cytotoxicity of Nanoparticulate Silver Bone Cement. *Biomaterials* **2004**, *25*, 4383−4391.
(18) Huang, W.; Sher, Y. P.; Peck, K.; Fung, Y. C. Matching Gene Activity with Physiological Functions. *Proc. Natl. Acad. Sci. U.S.A.* **2002**, *99*, 2603−2608.
(19) Liu, L.; Xu, K.; Wang, H.; Tan, P. K.; Fan, W.; Venkatraman, S. S.; Li, L.; Yang, Y. Y. Self-Assembled Cationic Peptide Nanoparticles as an Efficient Antimicrobial Agent. *Nat. Nanotechnol.* **2009**, *4*, 457−463.
(20) Hyde, A. J.; Parisot, J.; McNichol, A.; Bonev, B. B. Nisin-Induced Changes in *Bacillus* Morphology Suggest a Paradigm of Antibiotic Action. *Proc. Natl. Acad. Sci. U.S.A.* **2006**, *103*, 19896−19901.
(21) Zhao, Y.; Tian, Y.; Cui, Y.; Liu, W.; Ma, W.; Jiang, X. Small Molecule-Capped Gold Nanoparticles as Potent Antibacterial Agents That Target Gram-Negative Bacteria. *J. Am. Chem. Soc.* **2010**, *132*, 12349−12356.
(22) Hamilton-Miller, J. M.; Shah, S.; Smith, C. Silver Sulphadiazine: A Comprehensive in Vitro Reassessment. *Chemotherapy* **1993**, *39*, 405−409.